FEATURE ARTICLE

The Equation of State of an Energy Landscape

Pablo G. Debenedetti,*,† Frank H. Stillinger,‡,§ Thomas M. Truskett,† and Christopher J. Roberts†

Department of Chemical Engineering, Princeton University, Princeton, New Jersey 08544, Bell Laboratories, Lucent Technologies, Murray Hill, New Jersey 07974, and Princeton Materials Institute, Princeton University, Princeton, New Jersey 08544

Received: April 27, 1999; In Final Form: June 28, 1999

The topography of the multidimensional potential energy landscape is receiving much attention as a useful object of study for understanding complex behavior in condensed-phase systems. Examples include protein folding, the glass transition, and fracture dynamics in solids. The manner in which a system explores its underlying energy landscape as a function of temperature offers insight into its dynamic behavior. Similarly, sampling in density, in particular the relationship between the pressure of mechanically stable configurations and their bulk density (the equation of state of the energy landscape), provides fresh insights into the mechanical strength of amorphous materials and suggests a previously unexplored connection with the spinodal curve of a superheated liquid. Mean-field calculations show a convergence at low temperature between the superheated liquid spinodal and the pressure-dependent Kauzmann locus, along which the difference in entropy between a supercooled liquid and its stable crystalline form vanishes. This convergence appears to have implications for the glass transition. Application of these ideas to water sheds new light into this substance's behavior under conditions of low-temperature metastability with respect to its crystalline phases.

I. Introduction

Many of the most striking and provocative phenomena with which physical chemistry and materials science are concerned occur in condensed phases. Examples include the occurrence of metastable states and their destruction by nucleation or spinodal decomposition,[1] shock and detonation wave propagation,[2] protein folding from random-coil to native states,[3] spontaneous assembly of diverse mesoscopic structures,[4] and fracture dynamics of solid materials.[5] A feature common to all of these is the concerted, or cooperative, action of many molecular degrees of freedom subject to the molecular interactions that are present.

A full understanding of collective phenomena exhibited by condensed phases must account for the consequences of each constituent molecule constantly experiencing strong and often competing interactions with many neighbors. This situation has sown the seeds for germination and growth of a general "rugged landscape paradigm" for understanding condensed phase behavior, *i.e.*, a formal representation of many-molecule systems that focuses on the multidimensional potential energy hypersurface.[6,7] This Feature Article presents some recent results and thoughts that have emanated from this rugged landscape viewpoint. In particular, we concentrate on how the equation of state (including both equilibrium an metastable states) reveals some key aspects of the multidimensional potential energy landscape topography. As will be demonstrated below, this line of investigation goes to the fundamental questions concerning the nature of the liquid state and of the amorphous glasses that can be formed from supercooled liquids.

The following section II lays the groundwork for our presentation with the necessary basic definitions and statistical thermodynamic relations to establish the energy landscape representation. Section III considers the information that can be extracted by sampling the system at different temperatures under constant volume conditions; in particular we review and interpret results that have emerged form recent computer simulations on glass-forming binary mixtures.[8−10] Section IV examines the complementary case of sampling in density, which leads to the analysis of spinodal curves and to the issue of the mechanical strength of amorphous solids. Section V illustrates these phenomena with some mean-field calculations of the kind initiated some years ago by Longuet-Higgins and Widom,[11] but generalized here, and with implications for the density (or pressure) dependent Kauzmann temperature. Section VI applies these ideas to the case of water, showing connections to the complicated and still-debated properties of this substance's supercooled liquid and amorphous solid states at low temperature.[12−14] The final section, section VII, contains our views about the most productive future directions for the rugged landscape approach to open problems in physical chemistry and materials science.

II. Theoretical Background

We shall be concerned with material systems containing some macroscopic total number N of discrete particles (atoms, ions,

* Corresponding author.
† Department of Chemical Engineering.
‡ Bell Laboratories.
§ Princeton Materials Institute.

10.1021/jp991384m CCC: $18.00
Published on Web 08/10/1999

or molecules). In general N will include ν chemically distinguishable species present in respective numbers $N_1,...,N_\nu$,

$$N = \sum_{\alpha=1}^{\nu} N_\alpha \tag{2.1}$$

Each species of particle possesses a characteristic set of degrees of freedom that include center of mass position, and for polyatomics may also include rotational, vibrational, and conformational degrees of freedom. If these configurational degrees of freedom total $3 + n_\alpha$ for a particle of species α, the number of configurational degrees of freedom for the entire system is

$$D = \sum_{\alpha=1}^{\nu} (3 + n_\alpha) N_\alpha \tag{2.2}$$

The potential energy function for the system will be written $\Phi(\mathbf{X}|V)$. It contains interparticle interactions, wall potentials that confine the system to fixed volume V and intraparticle force fields, if any. The D-component configuration vector $\mathbf{X}$ is shorthand notation for the complete set of individual particle configuration vectors:

$$\mathbf{X} \equiv (\mathbf{x}_1, ..., \mathbf{x}_N) \tag{2.3}$$

The "energy landscape" cited in the title to this article refers to the geometry of the Φ hypersurface in the $(D+1)$-dimensional space of variables $\mathbf{X}$, Φ. Although our three-dimensional capacity to visualize topographic features has limited ability to cope with this high-dimensional geometry, the three-dimensional analogy and its intuitive suggestions are useful for understanding condensed-phase properties.

Some general remarks about Φ are in order. First, it is bounded below by a quantity proportional to the number of particles present:

$$\Phi \geq B(N_1/V, ..., N_\nu/V)N \tag{2.4}$$

Second, Φ is continuous and at least twice differentiable in all D configuration coordinates, provided all pairs of nuclei have nonzero separation. Third, Φ is invariant under permutation of identical particle species, and under operations corresponding to permanent symmetries of the particles (e.g., inversion of homonuclear diatomics).

Assuming that classical dynamics suffices to describe the system's time evolution, the Newtonian equations of motion determine the evolution of the configuration point $\mathbf{X}$ on the Φ hypersurface:

$$\mathbf{M}\cdot\ddot{\mathbf{X}}(t) = -\nabla_{\mathrm{X}}\Phi(\mathbf{X}) \tag{2.5}$$

where $\mathbf{M}$ is a diagonal matrix of appropriate masses. If the system is weakly coupled to a heat bath at sufficiently high temperature T, the motion of $\mathbf{X}(t)$ will explore the Φ hypersurface quasi-ergodically, *i.e.*, it will provide a dense and representative sampling of that hypersurface. This corresponds to a state of thermodynamic equilibrium for the given T and V, and thermodynamic properties can then be extracted from the canonical partition function:

$$Z(\beta, V) = \{\prod_\alpha N_\alpha![C_\alpha(\beta)]^{N_\alpha}\}^{-1} \int \exp[-\beta\Phi(\mathbf{X}|V)]\mathrm{d}^D\mathbf{X}$$
$$\equiv \exp[-\beta F(\beta, V)] \tag{2.6}$$

Here F is the Helmholtz free energy, and β is $(k_B T)^{-1}$. The configurational integrations cover the fixed volume V. The single-particle quantities C_α result from integration over conjugate momenta and depend only on T (not V); for monatomic particles they are cubes of mean thermal de Broglie wavelengths.

Steric repulsions dominate the interaction between any two atoms when they are sufficiently close. Consequently the physically relevant portions of the D-dimensional configuration space contributing to the integral in eq 2.6 avoid all severe atom-pair overlaps. It is then possible to show that only an exponentially small (in N) fraction of the full configuration space contributes significantly to Z, eq 2.6. The implied topographic vision thus conveyed for the physically relevant portion of the Φ hypersurface is that of a very sparse, steep-walled labyrinth threading across the $\mathbf{X}$ space.

Further elaboration of the rugged energy landscape rests upon identifying local minima of Φ and their surrounding "basins of attraction". These minima satisfy the relation

$$\nabla_{\mathrm{X}}\Phi = 0 \tag{2.7}$$

and are mechanically stable arrangements of the N particles in V that are often denoted "inherent structures" of the system.[7,15,16] The set of all configurations $\mathbf{X}(0)$ that continuously deform to a given inherent structure μ by steepest descent on the Φ hypersurface according to

$$\mathrm{d}\mathbf{X}(s)/\mathrm{d}s = -\nabla_{\mathrm{X}}\Phi[\mathbf{X}(s)|V] \quad s \geq 0 \tag{2.8}$$

defines the basin of attraction $\mathrm{B}(\mu)$ for μ. By means of this steepest descent mapping onto Φ minima, the entire configuration space becomes divided among (*i.e.*, tiled by) inherent structure basins.

Introduction of the inherent structures and their basins leads naturally to an alternative expression for $Z(\beta, V)$:

$$Z = \{\prod_\alpha C_\alpha^{-N_\alpha}\} \sum_\mu{}' \int_{B(\mu)} exp(-\beta\Phi)\mathrm{d}^D\mathbf{X} \tag{2.9}$$

Here we have taken advantage of permutational symmetry, so that the primed μ summation includes only one of each of the $\prod N_\alpha!$ equivalent inherent structures. Small displacements from the basin minimum can adequately be described as harmonic vibrations. Large excursions, particularly those that take the system near the transition states (saddle points) in the basin boundary entail substantial anharmonicity but can still validly be described as intrabasin "vibrational" displacements for that inherent structure.

It is useful to classify the inherent structures by their depths, *i.e.*, their Φ values on a per particle basis:

$$\varphi(\mu) = N^{-1}\Phi[\mathbf{X}(\mu)|V] \tag{2.10}$$

In the large system limit (fixed N/V) the depth-dependent density of distinct inherent structures possesses an asymptotic form exponential in N that we write as follows:[17]

$$exp[N\sigma(\varphi)] \qquad (\varphi_l \leq \varphi \leq \varphi_u) \tag{2.11}$$

where σ is nonnegative. As indicated, σ is defined strictly only between finite limits that correspond to the most stable (φ_l) and least stable (φ_u) inherent structures. This permits Z to be rewritten as a one-dimensional integral over the depth parameter φ:

$$Z = \{\prod_{\alpha} C_{\alpha}^{-N_{\alpha}}\} \int_{\varphi_l}^{\varphi_u} exp\{N[\sigma(\varphi) - \beta\varphi - \beta f^{(v)}(\beta,\varphi)]\} d\varphi \quad (2.12)$$

Here $f^{(v)}$ represents the mean intrabasin vibrational free energy per particle, for those basins whose depths lie in a narrow interval surrounding φ:

$$exp[-N\beta f^{(v)}(\beta,\varphi)] = \langle \int_{B(\mu)} \exp[-\beta\Delta\Phi(\mathbf{X})] d^D\mathbf{X} \rangle_{\varphi\pm\epsilon}, \quad \Delta\Phi(\mathbf{X}) = \Phi(\mathbf{X}) - \Phi[\mathbf{X}(\mu)] \quad (2.13)$$

For systems of macroscopic size, where N is comparable to Avogadro's number, the integral in eq 2.12 for Z is dominated by the immediate neighborhood of $\varphi^*(\beta, V)$, the position of the integrand maximum. This is located by the criterion

$$0 = (\partial/\partial\varphi)[\sigma(\varphi) - \beta\varphi - \beta f^{(v)}(\beta,\varphi)] \quad (2.14)$$

and so the large-system free energy per particle becomes

$$\beta F(\beta,V)/N = \sum_{\alpha} (N_{\alpha}/N) ln\, C_{\alpha}(\beta) - \sigma(\varphi^*) + \beta\varphi^* + \beta f^{(v)}(\beta,\varphi^*) \quad (2.15)$$

This expression makes clear the sense in which temperature variations sample different portions of the rugged potential energy landscape: as temperature varies, the corresponding changes in $\varphi^*(\beta,V)$ identify the depth of the basin subset that preferentially hosts the system configuration point $\mathbf{X}(t)$.

The pressure (p) equation of state follows from eq 2.15 by applying an isothermal volume derivative. Using the chain rule this leads to the following expression ($\rho = N/V$):

$$\beta p/\rho = -\left(\frac{\partial\sigma(\varphi^*,\rho)}{\partial \ln \rho}\right)_{\varphi^*} + \beta\left(\frac{\partial f^{(v)}(\beta,\varphi^*,\rho)}{\partial \ln \rho}\right)_{\beta,\varphi^*} + \left[-\left(\frac{\partial\sigma(\varphi^*,\rho)}{\partial\varphi^*}\right)_{\rho} + \beta + \beta\left(\frac{\partial f^{(v)}(\beta,\varphi^*,\rho)}{\partial\varphi^*}\right)_{\beta,\rho}\right]\frac{\partial\varphi^*}{\partial \ln \rho} \quad (2.16)$$

Phase transitions generally will produce singularities in all of σ, $f^{(v)}$, and φ^*.

The thermal equilibrium assumption under which all results thus far have been derived presumes that configuration point $\mathbf{X}(t)$ can explore the entire available configuration space. However, first-order phase changes (melting, freezing, boiling, condensation) can have very substantial kinetic nucleation bottlenecks that effectively block such full exploration on the laboratory, or simulation, time scale. Thus "equilibrated" metastable states can appear, for which $\mathbf{X}(t)$ is confined to, but densely explores, a subset of the complete available phase space. This confinement can equally well be described as involving only a subset of inherent structures and their basins.[18,19]

To illustrate this last point, consider specifically the liquid supercooled below its thermodynamic freezing point. The inherent structures for this metastable state are amorphous, *i.e.*, they are devoid of crystalline regions of any but the smallest size, too small in fact to support crystal nucleation. The crystallite-free amorphous inherent structures (denoted by subscript "a") and their basins are enumerated asymptotically with the analog of expression 2.11:

$$\exp[N\sigma_a(\varphi)] \qquad (\varphi_{la} \le \varphi \le \varphi_u), \quad \sigma_a(\varphi) \le \sigma(\varphi) \quad (2.17)$$

This subset has its own vibrational free energy $f_a^{(v)}(\beta, \varphi, \rho)$. The supercooled liquid above its glass transition temperature (to assure full relaxation) then has its free energy and pressure given by the same expressions as shown in eqs 2.15 and 2.16, respectively, but with σ, $f^{(v)}$, and φ^* replaced with σ_a, $f_a^{(v)}$, and φ_a^*.

III. Isochoric Temperature Sampling

Computer simulation studies in both molecular dynamics (MD) and Monte Carlo (MC) variants have been valuable information sources concerning potential energy landscapes. The typical procedure involves applying an inherent-structure-finding minimization routine at regularly spaced intervals within an equilibrated run. A variety of model systems have now been so analyzed and have revealed some initially unsuspected properties of φ^*, φ_a^*, and the associated inherent structures. In this section we review principal findings from constant-volume simulations for dense liquids.

Single-component nonassociated liquids present a consistent insightful pattern. This group includes monatomic models with additive pair potentials of the Lennard-Jones type:[20] those that, upon crystallization, produce body-centered cubic[21] and simple hexagonal[22] solids, and Gaussian[23] and inverse-power[24] potentials. It also includes a model for the diatomic halogen F_2 in which nonadditive interactions were present to enforce the correct chemical valency.[25] The common observation for all of these simple liquids at fixed density is that the mean inherent structure energy φ_a^* for the liquid state is virtually independent of temperature. This conclusion covers a wide range of liquid temperatures, typically from several times the melting temperature down to the moderately or even deeply supercooled regime.

This statistical invariance of inherent structure samples to liquid temperature is confirmed by examining pair correlation functions $g^{(2)}(r)$ for the states involved. Although $g^{(2)}$'s for the equilibrated liquids manifest substantial temperature dependence, those for the corresponding sets of inherent structures, $g_q^{(2)}$, are virtually identical to one another, exhibiting the same enhanced image of short-range order. The conclusion is that, for simple single-component liquids at least, temperature dependence of properties resides almost exclusively with intrabasin vibrational excitation.

From the energy landscape viewpoint, this observation indicates that the depth distribution function σ_a for simple liquids is quite narrow on the energy scale of $k_B T_m$, the thermal energy at the melting point for the given density. Although the potential energy hypersurface is indeed topographically rugged, its constituent basins do not vary greatly in altitude or in the local order of their minima. Assuming the same is true for interbasin transition-state saddle points, this is consistent with the fact that these simple liquids crystallize relatively easily (both experimentally and in simulations) upon cooling below T_m. There are few deep, trapping, amorphous basins to inhibit the dynamic exploration of the energy landscape that is necessary to find and to settle into crystalline basins.

Good glass formers present a rather different picture. One notable example is a binary Lennard-Jones system whose parameters have been selected to imitate the 80% Ni + 20% P alloy that exhibits a deep eutectic, and readily forms amorphous solids.[27,28] The potential parameters are the following:[8−10]

$$\epsilon_{AB} = 1.50\epsilon_{AA}, \quad \epsilon_{BB} = 0.50\epsilon_{AA}$$
$$\sigma_{AB} = 0.80\sigma_{AA}, \quad \sigma_{BB} = 0.88\sigma_{AA} \quad (3.1)$$

where A and B respectively stand for Ni and P. The reduced temperature (in ϵ_{AA}/k_B units) for the eutectic point is approximately 1.2, and the total number density (in σ_{AA}^{-3} units) is 1.20.

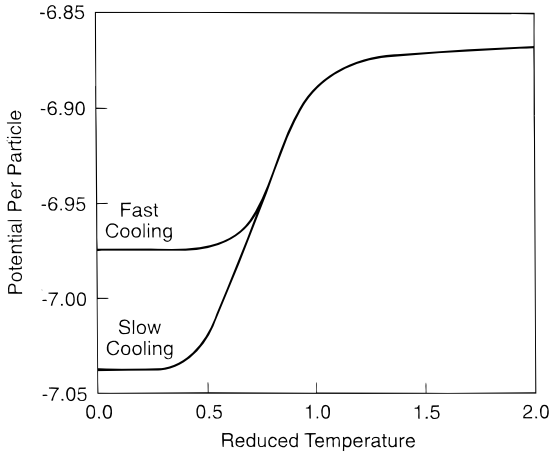

Figure 1. Mean inherent structure energy per particle vs initial liquid temperature for the binary Lennard-Jones system chosen to represent the $Ni_{80}P_{20}$ system. The cooling rates indicated differ by factor 324. Adapted from ref 10.

At high temperatures (above approximately 1.0 reduced units), φ_a^* is nearly independent of temperature, in conformity with the simple-liquid behavior discussed above. But as the temperature of the mixture declines below 1.0, φ_a^* displays a marked continuous dropoff, indicating that on account of favorable Boltzmann weighting the system has discovered and entered anomalously deep basins.[10] The cooling rate used in the simulation strongly influences the final basin depth: the slower the cooling, the deeper the basin. In no case has crystal nucleation been observed. Figure 1 schematically indicates these results. It remains an open question for this model what depth would be attained by "infinitely slow" cooling, *i.e.*, the potential energy of the most stable amorphous inherent structure.

Equation 2.14, applied to the amorphous basin subset to determine φ_a^*, can be used to interpret the pattern presented by Figure 1. Because the vibrational free energy depends only weakly on depth parameter φ, we have

$$\beta\varphi + \beta f_a^{(v)}(\beta,\varphi) \cong \beta\varphi + C(\beta) \tag{3.2}$$

i.e., a linear function of φ with slope β. Equation 2.14 requires that this combination and $\sigma_a(\varphi)$ have matching slopes at $\varphi_a^*(\beta)$. The pattern shown in Figure 1 then demands that σ_a be broadened at least to the low-φ side of its maximum, in contrast to the narrow distribution that obtains for simple liquids. Figure 2 illustrates these distinctive forms. Both cases exhibit high curvature at their maxima, which creates a nearly-constant φ_a^* plateau; the gentler slope for case 2b, the glass-formers, generates the drop shown in Figure 1.

Evidently the good glass formers enjoy a richer energy hypersurface topography compared to that of the simple liquids. Rare but significant regions of the configuration space exist that are occupied by clusters of anomalously deep amorphous basins. Their local topography appears to be exceptionally rugged, with interbasin transition states substantially higher than the minima they connect in comparison with the commoner basins and transition states sampled at high temperature. These are very effective traps for the system configuration point $\mathbf{X}(t)$ at low temperature, preventing crystal nucleation. The exceptional local ruggedness around these trapping regions presumably plays a central role in determining the distinctive non-Arrhenius and stretched-exponential flow and relaxation behavior of "fragile" glass formers.[28]

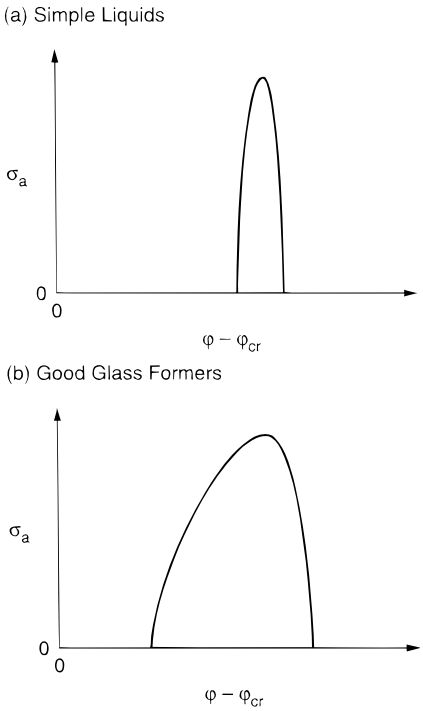

Figure 2. Characteristic distributions of basin depths (a) for simple liquids and (b) for liquids easily supercooled to form glasses. The absolute potential energy minimum (crystalline state) per particle has been denoted by φ_{cr}.

IV. Sampling in Density

Varying the system volume V can be expected to influence the character of the rugged potential energy landscape. In the event that all molecular interactions were proportional to a common inverse-power of distances, this influence would be describable by simple scaling laws, with no change in total number of basins.[29] More generally, each of σ, $f^{(v)}$, and φ^* (alternatively σ_a, $f_a^{(v)}$, and φ_a^*) would vary with V in ways characteristic of the specific substances involved. Recall that, in eq 2.16, differential changes in these quantities determine the pressure equation of state.

We have already emphasized that for simple liquids examined at constant density, the collections of inherent structures generated by steepest-descent quenching are virtually independent of liquid temperature. However it is instructive to examine how these temperature independent results vary with density. For this purpose we revisit a recent Monte Carlo simulation for a single-component fluid of particles ($N = 256$ and 1372) with smoothly truncated Lennard-Jones interactions.[20b] Figure 3 shows a plot of inherent structure pressure vs number density, over a moderately wide density range. For this model the critical and triple point reduced densities $\rho\sigma^3$ are approximately 0.25 and 0.67, respectively.[19] The results shown are continuous and smooth, but unambiguously nonmonotonic.

Three density intervals have been distinguished in Figure 3.

$$\begin{aligned} &\text{A:} \quad 0.99 < \rho\sigma^3 \\ &\text{B:} \quad 0.89 < \rho\sigma^3 < 0.99 \\ &\text{C:} \quad \rho\sigma^3 < 0.89 \end{aligned} \tag{4.1}$$

The first of these (A) has inherent structures at positive pressure; the dense liquids from which they were generated exhibited even larger positive pressures. Interval B has inherent structures that are in a state of tension (*i.e.*, negative pressure) that is largest

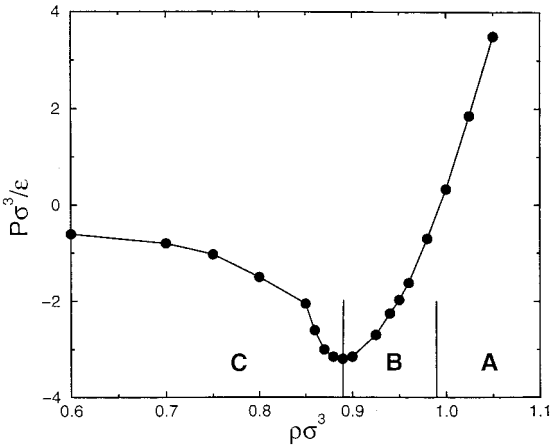

Figure 3. Density variation of inherent structure pressure for a fluid with a smoothly truncated Lennard-Jones pair potential (ref 20b).

in magnitude at its lower density endpoint,

$$\rho_s\sigma^3 = 0.89 \tag{4.2}$$

Interval C shows monotonic reduction in the inherent structure tension as density declines even further. This pattern was first observed by La Violette.[20a]

Geometric analysis[20b] of the inherent structures represented in Figure 3 confers a singular significance on density ρ_s. It is the point below which attractive interparticle forces are unable mechanically to sustain the system as an amorphous, isotropic, and spatially homogenous medium. Expanding the system to lower densities fractures, or shreds, the inherent structures so that they consist of dense amorphous portions threaded by large pores or cavities. In this fractured state it is not surprising that less and less tension exists as density decreases.

Although even lower densities than those indicated in Figure 3 have not been examined yet, the rational expectation is that inherent structure tensions would continue to decline toward zero, while their structures become more and more tenuous, like "aerogels".[30]

The smooth pressure vs density curve with a well-developed minimum is reminiscent of the metastable pressure isotherms within phase coexistence regions that are predicted by the van der Waals and other approximate equations of state.[31] In fact we argue that this inherent structure curve is the natural zero-temperature limit of such metastable isotherms, at least for simple liquids. In particular we claim that the minimum shown in Figure 3 is the zero-temperature limit of the liquid spinodal curve.[32] This identification receives support from the mean-field calculations reported in the following section V. One should note in passing that the negative-compressibility "unstable" portion of the van der Waals-like isotherms, conventionally described as unattainable,[33] possesses tangible form in interval C because the inherent structures contain no thermal motion by construction.

An analogous but more elaborate situation arises for good glass formers. As noted earlier (section III), the mean cohesive energy for inherent structures in these systems shows a significant, and characteristic, dependence on the temperature of the liquids. So too will the mean pressures exhibited by the inherent structures depend on the liquid temperature. Consequently we can anticipate that the single temperature-independent curve of Figure 3 will be replaced by a family of curves, indexed by temperature, for good glass-forming materials. In particular the density ρ_s and its associated negative pressure should depend on liquid temperature. Although it has not (to the best of our knowledge) yet been tested experimentally, a reasonable prediction seems to be that the lower the temperature, the stronger the inherent structures will be at resisting tension-induced fracture; consequently, we predict that the most negative pressures (at ρ_s) will occur for the most deeply supercooled and equilibrated glass formers.

V. Mean Field Calculations

The venerable van der Waals equation of state,[31]

$$\frac{\beta p}{\rho} = \frac{1}{1-b\rho} - \beta a\rho \tag{5.1}$$

containing positive constants a and b, provides a qualitatively correct description of vapor, liquid, and critical region behaviors, as well as the coexistence region connecting them. It does so by accounting approximately for the effects of repulsive and of attractive intermolecular forces, respectively, through the first and second terms in the right member of eq 5.1. One of its primary shortcomings is failure to account for the existence of the crystalline solid.

Longuet-Higgins and Widom reactivated the original van der Waals ideas in a more modern setting.[11] They observed that the repulsive-force term in eq 5.1 could be replaced by an accurate form appropriate for hard spheres, while retaining the attractive-force term as a mean-field approximation that is formally exact in the long-range-attraction limit. The presence of a first-order melting/freezing transition in the bare hard sphere system[34] then maps into a corresponding transition when attractions are present; furthermore, an improved description of dense liquids emerges.

The Longuet-Higgins, Widom approach offers a useful tool to investigate the connections discussed above (section IV) between inherent structures and spinodal curves, at least for simple liquids. It should be emphasized that their important approach can now be generalized to incorporate other repulsive-particle models beyond simple hard spheres. Specifically, the cases of "diatomic" fused spheres[35] and of "soft spheres"[24,36] are now well-enough studied and characterized in their own rights to serve as alternate, and possibly more realistic, versions of the repulsive force model.

For this presentation we will focus on a specific soft-sphere model as a reasonable representation of interatomic repulsions. The potential energy of interaction has the following form:

$$\Phi_0(\mathbf{r}_1...\mathbf{r}_N) = \epsilon\sum_{i<j}(\sigma/r_{ij})^9 \tag{5.2}$$

It is well-known that inverse-power potentials such as this produce classical equations of state (and other thermodynamic attributes) that depend on a single scaling variable.[36] The relevant variable z for the inverse-ninth-power case, eq 5.2, is

$$z = (\beta\epsilon)^{1/3}\rho\sigma^3 \tag{5.3}$$

The pressure p_0 and energy E_0 for this soft-sphere model then depend on a single function of z:

$$\frac{\beta p_0}{\rho} = 1 + u(z) \tag{5.4}$$

$$\frac{\beta E_0}{N} = \frac{3}{2} + \frac{u(z)}{3} \tag{5.5}$$

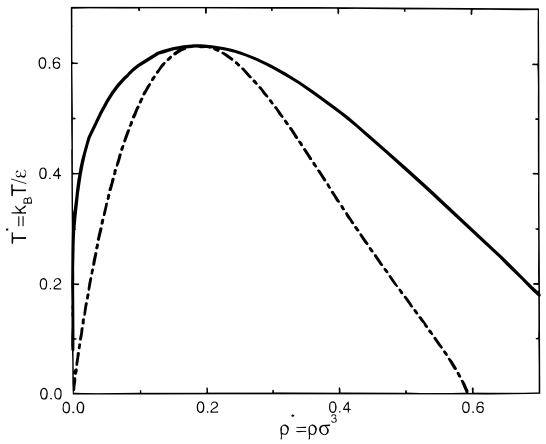

Figure 4. Binodal (solid) and spinodal (dash−dot) curves for the soft-sphere plus mean-field equation of state eq 5.8. Coupling constant $a = 5\epsilon\sigma^3$.

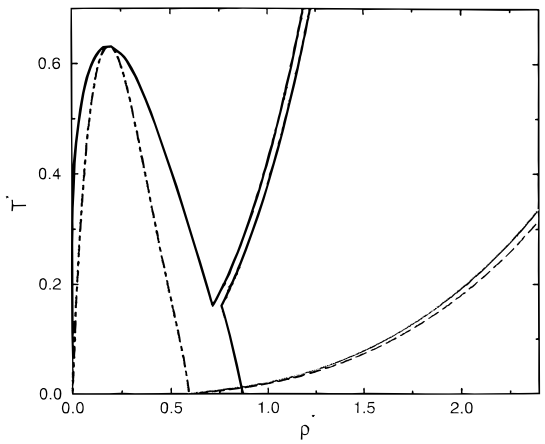

Figure 5. Repeat of the liquid−vapor binodal and spinodal curves of Figure 4, along with the binodal curves for solid−liquid equilibrium, for the soft-sphere plus mean-field equation of state, eqs 5.6b, 5.8, 5.10. Also shown are the Kauzmann curves for the liquid (solid) and the crystal (dashed). The crystal and liquid phases along the Kauzmann curves have the same entropy at the given temperature (shown) and pressure (not shown).

The function $u(z)$ can be viewed as consisting of two branches, $u_f(z)$ and $u_c(z)$, representing fluid and crystal phases respectively. The former has a convergent power series in z that generates virial expansions for eqs 5.4 and 5.5. In the large-z asymptotic regime one can show that

$$u_f(z) \sim 3\varphi_a z^3 + 9/2 + 0(z^{-3}) \tag{5.6a}$$

$$u_c(z) \sim 3\varphi_c z^3 + 9/2 + 0(z^{-3}) \tag{5.6b}$$

Here dimensionless constants φ_a and φ_c are determined by the mean inherent structure energies for the amorphous fluid and periodic crystal phase and are known from molecular dynamics simulation to have the numerical values:[37]

$$\varphi_a \cong 2.3784$$

$$\varphi_c \cong 2.2084 \tag{5.7}$$

Following Longuet-Higgins and Widom,[11] the soft-sphere version of van der Waals eq 5.1 is

$$\beta p/\rho = 1 + u(z) - \beta a\rho \tag{5.8}$$

The spinodal curves correspond to infinite isothermal compressibility, which for eq 5.8 occurs when

$$0 = 1 + u_f(z) + zu'_f(z) - 2\beta a\rho \tag{5.9}$$

Data from a molecular dynamics simulation for the soft-sphere model[37] permits determination of a smooth fit function for u_f, which approaches eq 5.6a in the large-z limit:

$$u_f(z) = 7.13524z^3 + \frac{1.72138z}{3.37366 + z} + \frac{3.42602z + 2.77862z^2}{1.473 - 0.857z + z^2} \tag{5.10}$$

This equation, along with eq 5.8, has been used to find the spinodal and binodal (liquid−vapor coexistence) curves (Figure 4). For the mean-field coupling parameter choice $a = 5\epsilon\sigma^3$, the liquid-branch spinodal approaches $\rho\sigma^3 = 0.592$, $p\sigma^3/\epsilon = -0.8759$ as $T \to 0$. Note that the theory defined by eqs 5.2 and 5.8 is a two-parameter theory. The natural choice of parameters is a and $(\epsilon\sigma^9)$. However, if one chooses ϵ and σ as scaling parameters, as we do in Figures 4 and 5, one is forced to specify the ratio $(a/\epsilon\sigma^3)$ independently. However, the results presented below in eqs 5.12 and 5.13 are general and do not require specifying $(a/\epsilon\sigma^3)$.

The metastable pressure isotherm in the zero temperature limit can be extracted from eq 5.8, using eq 5.6a. The result is the following:

$$(p\sigma^3/\epsilon)_{T=0} = 3\varphi_a(\rho\sigma^3)^4 - (a/\epsilon\sigma^3)(\rho\sigma^3)^2 \tag{5.11}$$

This expression generates curves qualitatively like that shown earlier in Figure 3 for Monte Carlo simulation. In particular it leads to a single minimum located at

$$\rho_s\sigma^3 = (a/6\varphi_a\epsilon\sigma^3)^{1/2}$$

$$p_s\sigma^3/\epsilon = -(1/12\varphi_a)(a/\epsilon\sigma^3)^2 \tag{5.12}$$

These are the mean-field estimates for the density and maximum tensile strength of amorphous packings for inverse-ninth-power soft spheres with long-range attractions, given an arbitrary positive value of a. Other choices for the inverse power would yield similar, but shifted, expressions.

Comparing results from eq 5.12 with corresponding quantities at the liquid−vapor critical point (cp) helps to put the mechanical-strength aspect of the energy landscape in a more familiar context. One finds

$$\rho_s/\rho_{cp} \cong 3.13$$

$$p_s/p_{cp} \cong -20.75 \tag{5.13}$$

These values are similar to those that obtain for the smoothly truncated Lennard-Jones system[19,20b] upon which Figure 3 is based:

$$\rho_s/\rho_{cp} \cong 3.6$$

$$p_s/p_{cp} \cong -30 \tag{5.14}$$

The same ratios can also be deduced for the van der Waals equation of state:

$$\rho_s/\rho_{cp} = 3 \tag{5.15}$$

$$p_s/p_{cp} = -27 \tag{5.15}$$

Figure 5 once again shows the liquid−vapor binodal and spinodal curves from Figure 4, the solid−liquid coexistence curves, and the computed "Kauzmann curve". This last locus identifies the metastable liquid states which have the same entropy as the crystal, when the latter has the same temperature and pressure as the former. In order to generate this Kauzmann curve for the soft-sphere plus mean-field-attraction model, it is necessary to compute the free energy of the liquid and the crystal, from which the entropy is obtained by differentiation. The free energy of the reference soft-sphere fluid is obtained by integrating its equation of state (eqs 5.4 and 5.10) along a reversible path to the dilute gas phase. Likewise, the free energy of the soft-sphere crystal is computed by integration of the equation of state (eqs 5.4 and 5.6b). The integration constant is computed by requiring equality of chemical potential between the phases at the liquid−solid transition which has previously been located by computer simulation.[36] Following Longuet-Higgins and Widom,[11] a mean-field attraction term, $-a\rho$, is appended to the free energy of both phases.

The striking feature illustrated by Figure 5 is that, in the limit of absolute zero temperature, the Kauzmann curve appears to terminate at the same limit for the liquid spinodal. This is the mechanical strength limit identified earlier for homogeneous amorphous deposits, the minimum in the curves of type shown in Figure 3. The existence of this coincidence adds significance to the critically stretched glass state. Two further observations should be noted. First, the $T = 0$ stretched crystal corresponding to the terminus of the Kauzmann curve for this mean-field calculation is slightly more dense than its equal-entropy amorphous partner. Second, the qualitative pattern presented by Figure 5 also appears in the Longuet-Higgins and Widom hard-sphere and hard-disk plus mean-field-attraction models,[11,38] as well as in the analogous hard-dumbell case.[38] The presently available evidence suggests that this may be a generally applicable behavior, at least within the domain of classical statistical mechanics.

VI. Energy Landscape for Water

We now turn to consider briefly a case with obvious importance, namely water. The nonspherical molecules involved, and their capacity to engage in directional hydrogen bonds control the unusual properties of this substance, and present challenges for theoretical interpretation. The existence of many crystalline ice polymorphs[39] and clathrate networks,[40] as well as that of high- and low-density amorphous solids,[14] provides experimental testimony for the great diversity of inherent structures possible for water.

Yet in spite of the molecular complexity of the condensed phases of water, the substance shows similarity to the cases considered above. In particular, it displays (at least in model calculations) a characteristic density ρ_s of maximal mechanical stretch for its amorphous inherent structures. Figure 6 contains results for inherent structure average pressures, verses density, for a series of molecular dynamics simulations[41] using the well-tested SPC/E potential model for water.[42] Two curves are shown, corresponding to 400 K and to 260 K as the choices of liquid temperature from which the inherent structures were identified. Both pass through negative pressure minima, with density equal to about 0.88 g/cm^3. The fact that the two curves do not superpose shows that water (in this SPC/E model at least) exhibits temperature dependence at fixed density for its inherent structures. Indeed the simulations show that the 260 K inherent structures (lower curve in Figure 6) have consistently greater binding energy than the 400 K inherent structures (upper curve).

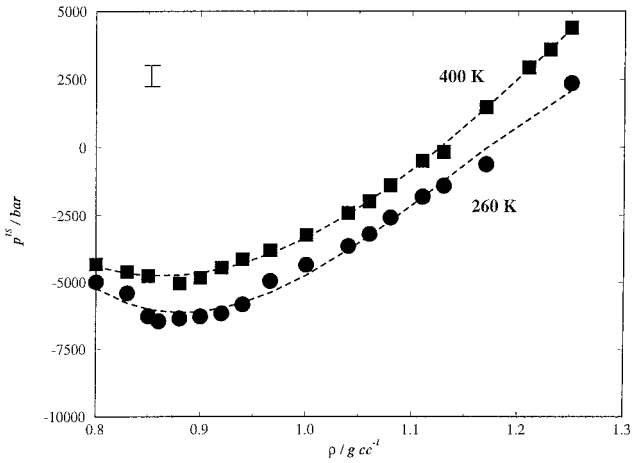

Figure 6. Density dependence of inherent structure pressures, p^{IS}, for the SPC/E model of liquid water. The two curves shown are labeled by the liquid temperature from which the inherent structures were prepared by constant-density quenching.

In this respect water behaves in a manner similar to the good glass formers discussed in section III above. It is also consistent with the recent claim[43] that in this temperature range liquid water behaves as a very fragile glass former. From the energy landscape viewpoint, it indicates that an exceptionally rugged and diverse topography exists for water.

The data presented in Figure 6 does not extend to low density. However a quick survey of the inherent structure spatial pattern at low density has been undertaken.[41] This confirms the presence of large voids or cracks analogous to the behavior mentioned above for the simpler Lennard-Jones models.

The existence of a Kauzmann curve for water, and its possible relation to the pressure minimum in Figure 6, remains a fascinating unexplored subject. Indeed this issue is complicated somewhat by the existence of several high-pressure ice polymorphs.[39] Nevertheless one might reasonably postulate that the Kauzmann curve constructed for the liquid and the familiar proton-disordered hexagonal ice *Ih* would terminate at the minimum of the 0 K spinodal curve.

VII. Conclusions and Discussion

Examples cited above demonstrate the deep connections, for condensed-phase substances, between macroscopic measurables embodied in the equation of state, and the multidimensional topography of the potential energy hypersurface that is created by molecular interactions. These connections are revealed by systematic application of constant-volume steepest-descent quenching to both stable and metastable thermal states of the substance of interest. The resulting collections of inherent structures (potential energy minima) reveal characteristic topographical differences between simple liquids, and good (fragile) glass formers. They also confer tangible form on the $T = 0$ K limit of the metastable pressure isotherm within the liquid−vapor coexistence region. The minimum in this isotherm locates the $T = 0$ limit of the liquid spinodal and corresponds to the mechanical stability limit (under isotropic tension) for amorphous, isotropic, spatially homogeneous glasses. Furthermore, this minimum also serves as the $T = 0$ K limit of the Kauzmann curve which locates the pressure-temperature point of entropy equality between liquid and crystal phases.

Thus, the zero-temperature limit of the liquid spinodal establishes a cutoff density below which a homogeneous glass cannot be formed. It also anchors the Kauzmann curve. The linearity of this curve in the (P, T) plane[44] implies simple

relations between the glass transition and Kauzmann temperatures. Furthermore, the maximum tension which the amorphous system can withstand emerges as an important scaling parameter in determining the slope of the $T_g(P)$ curve. The testing of these predictions against experimental observations for real materials is underway.

On account of the complexity of this general subject, but limited space for this presentation, we have confined attention to static properties of condensed phases. However, examining selected kinetic features adds additional detail to the topographic "energy landscape" picture.[10] In particular, rates of relaxation processes can be examined both for prequench and postquench versions of the system kinetics to probe barrier heights separating inherent structures.

In spite of the intriguing results obtained so far, many open issues remain. These include application to long-chain molecules and polymers, and to liquid crystal materials. Section VI has pointed out the need to locate and to interpret the Kauzmann curve for water; it will also be informative to search for connections to the curve of density maxima for liquid water. Finally, the role of quantum corrections to classical statistical mechanics in the energy landscape picture demands clarification.

Acknowledgment. P.G.D. gratefully acknowledges the support of the U.S. Department of Energy, Division of Chemical Sciences, Office of Basic Energy Sciences (Grant DE-FG02-87ER13714), and of the donors of the Petroleum Energy Fund, administered by the American Chemical Society. T.M.T. and C.J.R. acknowledge the National Science Foundation for Graduate Fellowships.

References and Notes

(1) Debenedetti, P. G. *Metastable Liquids*; Princeton University Press: Princeton, NJ, 1996.
(2) Cooper, P. W.; Kurowski, S. R. *Introduction to the Technology of Explosives*; VCH Publishers: New York, 1996.
(3) Gierasch, L. M.; King, J.; Eds. *Protein Folding*; American Association for the Advancement of Science: Washington, DC, 1990.
(4) Kim, S. S.; Zhang, W.; Pinnavaia, T. J. *Science* **1998**, *282*, 1302.
(5) Cramer, J.; Wanner, A.; Gumbsch, P. *Phys. Status Solidi* **1997**, *164*, R5.
(6) Frauenfelder, H., et al.; Eds. *Landscape Paradigms in Physics and Biology*; North-Holland: New York, 1997.
(7) Stillinger, F. H.; Weber, T. A. *Science* **1984**, *225*, 983.
(8) Weber, T. A.; Stillinger, F. H. *Phys. Rev. B* **1985**, *32*, 5402.
(9) Kob, W.; Andersen, H. C. *Phys. Rev. E* **1995**, *51*, 4626.
(10) Sastry, S.; Debenedetti, P. G.; Stillinger, F. H. *Nature* **1998**, *393*, 554.
(11) Longuet-Higgins, H. C.; Widom, B. *Mol. Phys.* **1964**, *8*, 549.
(12) Fourkas, J. T.; Kivelson, D.; Mohanty, U.; Nelson, K. A.; Eds.; *Supercooled Liquids, Advances and Novel Applications*; American Chemical Society Symposium Series 676; American Chemical Society: Washington, DC, 1997; Chapters 16−21.
(13) Rebelo, L. P. N.; Debenedetti, P. G.; Sastry, S. *J. Chem. Phys.* **1998**, *109*, 626.
(14) Mishima, O.; Stanley, H. E. *Nature* **1998**, *396*, 329.
(15) Patashinski, A. Z.; Ratner, M. A. *J. Chem. Phys.* **1997**, *106*, 7249.
(16) Somer, F. L., Jr.; Canright, G. S.; Kaplan, J. *Phys. Rev. E* **1998**, *58*, 5756.
(17) Stillinger, F. H. *Phys. Rev. E* **1999**, *59*, 48.
(18) Stillinger, F. H. *J. Chem. Phys.* **1988**, *88*, 7818.
(19) Corti, D. S.; Debenedetti, P. G.; Sastry, S.; Stillinger, F. H. *Phys. Rev. E* **1997**, *55*, 5522.
(20) (a) La Violette, R. A. *Phys. Rev. B* **1989**, *40*, 9952. (b) Sastry, S.; Debenedetti, P. G.; Stillinger, F. H. *Phys. Rev. E* **1997**, *56*, 5533.
(21) Weber, T. A.; Stillinger, F. H. *J. Chem. Phys.* **1984**, *81*, 5089.
(22) LaViolette, R. A.; Stillinger, F. H. *J. Chem. Phys.* **1985**, *82*, 3335.
(23) Stillinger, F. H.; Stillinger, D. K. *Phys. A* **1997**, *244*, 358.
(24) Stillinger, F. H.; Weber, T. A. *J. Chem. Phys.* **1985**, *83*, 4767.
(25) Stillinger, F. H.; Weber, T. A. *J. Chem. Phys.* **1988**, *88*, 5123.
(26) Cargill, G. S., III *J. Appl. Phys.* **1970**, *41*, 12.
(27) Dixmier, J.; Doi, K.; Guinier, A. In *Physics of Non-Crystalline Solids*; Prins, J. A., Ed.; North-Holland: Amsterdam, 1965; p 67.
(28) Stillinger, F. H. *Science* **1995**, *267*, 1935.
(29) Stillinger, F. H.; Debenedetti, P. G. *J. Phys. Chem. B* **1999**, *103*, 4052.
(30) Fricke, J. *Sci. Am.* **1988**, *258*, 92.
(31) Hirschfelder, J. O.; Curtiss, C. F.; Bird, R. B. *Molecular Theory of Gases and Liquids*; John Wiley and Sons: New York, 1954, p 250.
(32) Debenedetti, P. G. *Metastable Liquids*; Princeton University Press: Princeton, NJ, 1996; p 69.
(33) Guggenhein, E. A. *Thermodynamics*, 2nd ed.; Interscience Publishers: New York, 1950; p 131.
(34) Hoover, W. G.; Ree, F. H. *J. Chem. Phys.* **1968**, *49*, 3609.
(35) Tildesley, D. J.; Street, W. B. *Mol. Phys.* **1980**, *41*, 85.
(36) Hoover, W. G.; Gray, S. G.; Johnson, K. W. *J. Chem. Phys.* **1971**, *55*, 1128.
(37) Stillinger, F. H.; Stillinger, D. K. Unpublished results.
(38) Truskett, T. M. Unpublished results.
(39) Eisenberg, D.; Kauzmann, W. *The Structure and Properties of Water*; Oxford University Press: New York, 1969; Chapter 3.
(40) Davidson, D. W. In *Water, a Compreshensive Treatise*; Franks, F., Ed.; Plemum Press: New York, 1973; Vol. 2, Chapter 3.
(41) Roberts, C.; Debenedetti, P. G.; Stillinger, F. H. *J. Phys. Chem.* B **1999**. Submitted for publication.
(42) Ito, K.; Moynihan, C. T.; Angell, C. A. *Nature* **1999**, *398*, 492.
(43) Berendsen, H. J. C.; Grigera, J. R.; Straatsma, T. P. *J. Phys. Chem.* **1987**, *91*, 6269.
(44) Truskett, T. M.; Debenedetti, P. G.; Stillinger, F. H. In preparation.